RSC Advances

PAPER

View Article Online
View Journal | View Issue

Cite this: *RSC Adv.*, 2018, **8**, 38883

Structure and luminescence properties of $La_6Ba_4(SiO_4)_6F_2:Dy^{3+}$ phosphor with apatite structure

Jialei Zhang,[ab] Qingfeng Guo,*[ab] Libing Liao,*[c] Yongjie Wang,[d] Mingyue He,[ab] Huan Ye,[ab] Lefu Mei,*[c] Haikun Liu,[c] Tianshuai Zhou[c] and Bin Ma[e]

Received 8th October 2018
Accepted 24th October 2018

DOI: 10.1039/c8ra08324j

rsc.li/rsc-advances

In this study, we investigated the structure, luminescence properties and morphology of $La_6Ba_4(SiO_4)_6F_2:Dy^{3+}$ in detail using X-ray diffraction (XRD), photoluminescence spectroscopy, scanning electron microscopy (SEM) and decay kinetics measurements. The results indicate that $La_6Ba_4(SiO_4)_6F_2:Dy^{3+}$ was well crystallized, and its structure is of apatite-type and belongs to the hexagonal system. The prepared samples exhibit two intense characteristic bands in the blue (484 nm) and yellow (579 nm) spectral ranges corresponding to the Dy^{3+} transitions $^4F_{9/2} \rightarrow {}^6H_{15/2}$ and $^4F_{9/2} \rightarrow {}^6H_{13/2}$, respectively. These dominant photoluminescence bands are accompanied by a weak red band (670 nm) due to the $^4F_{9/2} \rightarrow {}^6H_{11/2}$ transition. The emission color of $La_6Ba_4(SiO_4)_6F_2:Dy^{3+}$ phosphors are found to fall in the white light region. The Dy^{3+} optimal dopant concentration in the $La_6Ba_4(SiO_4)_6F_2$ host was found to be 0.12 (mol). In addition, the phosphors have high thermal stability. Hence, $La_6Ba_4(SiO_4)_6F_2:Dy^{3+}$ may have an application in white light-emitting diodes.

1. Introduction

In the present time, white light-emitting diodes (w-LEDs) are being widely applied in the field of lighting because of their excellent characteristics, such as good reliability, low power consumption, long lifetime, environmental friendliness and high luminous efficiency.[1–3] By combining a yellow emitting phosphor such as YAG:Ce^{3+} and a blue LED, or by combining several different phosphors, w-LEDs can generally be fabricated.[4–7] However, they may have disadvantages associated with complicated phosphors such as efficiency loss. Respectively, the exploration of developing single-phase phosphors is a relevant task. Energy transfer of a single-phase host is an effective way to obtain white light, for example, $Sr_3Y_2(Si_3O_9)_2:Ce^{3+}$, Tb^{3+}/Mn^{2+}/Eu^{2+} phosphors[8] and $Sr_3Gd_2(Si_3O_9)_2:Ce^{3+}$, Tb^{3+}/Mn^{2+} phosphors.[9] In our study, we tried to use single Dy^{3+} doped phosphor to obtain white light in a more convenient manner than co-doped ones.

There is an abundance of f-block energy levels in Dy^{3+} with $^4f_9$ configuration. Strong emission is possible over the visible range,[10] consisting of three predominant emission bands in the blue region of 470–500 nm, yellow region of 550–600 nm and red region of 600–700 nm generated by the $^4F_{9/2} \rightarrow {}^6H_{15/2}$, $^4F_{9/2} \rightarrow {}^6H_{13/2}$ and $^4F_{9/2} \rightarrow {}^6H_{11/2}$ transitions, respectively.[11–13] Concentration of the Dy^{3+} ion as well as pump wavelength can have a pronounced impact on the intensity ratio of the yellow-blue emission (Y/B). This is due to the fact that the hypersensitive $^4F_{9/2} \rightarrow {}^6H_{13/2}$ transition has a strong intensity dependent on the host, whereas the $^4F_{9/2} \rightarrow {}^6H_{15/2}$ transition is less sensitive.[14] Thanks to this feasibility, the emission near white light is possible by adjusting the Y/B value.[15] Single-phased white-light-emitting phosphors doped by Dy^{3+} ions have been widely investigated, for instance, $Ca_9La(PO_4)_5(SiO_4)F_2:Dy^{3+}$,[16] $K_2Gd(PO_4)(WO_4):Dy^{3+}$,[17] $Na_3Sc_2(PO_4)_3:Dy^{3+}$,[18] $Sr_3Y(PO_4)_3:Dy^{3+}$ (ref. 19) and $Ca_3Si_2O_7:Dy^{3+}$.[20]

Compounds with apatite structure are considered as practical host materials because they have exceptional thermal and chemical stability.[21,22] Apatite-type compounds crystallize in the space group of $P6_3/m$ ($Z = 2$) and have a general chemical composition of $A_{10}[XO_4]_6Z_2$,[23] where A stands for divalent cations such as Ca^{2+}, Mg^{2+}, Ba^{2+} and Sr^{2+}; XO_4 represents a tetrahedron group in which X can be P, Si, Ge, V; Z can be anions such as OH^-, Cl^-, O^{2-}, F^-.[24–26] By isomorphic substitution, the A site can be occupied by rare earth ions like Y^{3+}, La^{3+}, Gd^{3+} or alkali metal ions like Li^+, Na^+, K^+.[27–29] Accordingly, we

[a]School of Gemology, China University of Geosciences, Beijing 100083, China. E-mail: qfguo@cugb.edu.cn
[b]Jewelry and Mineral Materials Laboratory of Experimental Teaching Demonstration Center, Beijing, China
[c]Beijing Key Laboratory of Materials Utilization of Nonmetallic Minerals and Solid Wastes, National Laboratory of Mineral Materials, School of Materials Sciences and Technology, China University of Geosciences, Beijing 100083, China. E-mail: clayl@cugb.edu.cn; mlf@cugb.edu.cn
[d]Institute of Physics, Polish Academy of Sciences, Al. Lotnikow 32/46, Warsaw 02-668, Poland
[e]Qinghai Provincial Key Laboratory of New Light Alloys, Qinghai Provincial Engineering Research Center of High Performance Light Metal Alloys and Forming, Qinghai University, Xining 810016, PR China

can skillfully design novel Dy^{3+}-doped phosphors with more accomplished light output for solid state lighting applications.

Being a likely host for the generation of tunable solid-state lasers and ultra-short pulses, the apatite-type $La_6Ba_4(SiO_4)_6F_2$ (abbreviated here as LBSF) compound was considered carefully.[30] There are two cationic sites in this compound, *i.e.*, C_3 point symmetry in 9-fold coordinated 4f sites and C_s point symmetry in 7-fold coordinated 6h sites.[31] Besides, numerous species of rare earth ions can be accepted in both sites.[32] In our previous studies, we have obtained emission-tunable (from blue to green) phosphor $La_6Ba_4(SiO_4)_6F_2$:Ce^{3+}, Tb^{3+} (ref. 33) and reddish-orange phosphor $La_6Ba_4(SiO_4)_6F_2$:Sm^{3+},[31] which further indicates that LBSF is an excellent host material for single-phased white light-emitting phosphors. However, LBSF:Dy^{3+} phosphors have not yet been reported. Hence, in this contribution, the systematic study of the synthesis, structure and luminescence properties of LBSF:Dy^{3+} phosphors are reported. We show that, having feasible application, $La_6Ba_4(SiO_4)_6F_2$:Dy^{3+} phosphors may act as a white-light-emitting phosphor for w-LEDs (white light-emitting diodes).

2. Experimental details

2.1. Synthesis

$La_{6-x}Ba_4(SiO_4)_6F_2$:xDy^{3+} (x = 0.03, 0.09, 0.12, 0.15, 0.18 and 0.30) compounds were synthesized using a high-temperature solid-state reaction method. La_2O_3 (Aldrich, 99.995%), $BaCO_3$ (Aldrich, 99.9%), SiO_2 (Aldrich, 99.9%), NH_4HF_2 (Aldrich, 99.9%) and Dy_2O_3 (Aldrich, 99.995%) were used as starting materials. The reagents were mixed and then ground, based on the calculated stoichiometric ratio. NH_4HF_2 was used with 50% stoichiometric excess to compensate for fluorine loss at high temperatures. The mixtures were well ground in an agate mortar, inserted into the alumina crucibles and pre-heated at 750 °C for 1 h in the air atmosphere. Afterwards, the precursors were ground and annealed at 1350 °C for 4 h in the air atmosphere. As-synthesized samples were cooled to room temperature (RT) and ground to powders for structural and optical characterizations.

2.2. Characterization

The structural properties of synthesized samples were carried out by X-ray powder diffraction using an XD-3, PGENERAL, China, with Cu Kα radiation (λ = 0.15406 nm), in the 2θ range from 10° to 70°, operating at 40 kV and 40 mA. Using a GeminiSEM 500 instrument for morphological characterization, the $La_6Ba_4(SiO_4)_6F_2$:xDy^{3+} (x = 0.12 mol) sample was examined by SEM. The photoluminescence (PL) and excitation (PLE) spectra of the samples were recorded with an F-4600 fluorescence spectrophotometer (HITACHI, Japan) equipped with a photomultiplier tube operating at 500 V and a 150 W Xe lamp as the excitation source. Decay kinetics measurements were performed at RT using a Spectrofluorometer (Horiba, Jobin Yvon TBXPS) with a tunable pulse laser radiation as an excitation source.

3. Results and discussion

3.1. Structure

The crystal structure and phase purity of the as-prepared phosphors were analyzed by XRD. In Fig. 1(a), XRD patterns of $La_{6-x}Ba_4(SiO_4)_6F_2$:xDy^{3+} (x = 0.03, 0.09, 0.12, 0.15, 0.18 and 0.30) phosphors are shown. The relative intensity and position of all diffraction peaks can be exactly matched with those of the $La_6Ba_4(SiO_4)_6F_2$ (ICSD no. 170852) standard,[34] revealing the formation of hexagonal $La_6Ba_4(SiO_4)_6F_2$-type compounds and showing that the small doped Dy^{3+} contents has not affected the pure phase composition. No other crystalline phases were detected. The view of $La_6Ba_4(SiO_4)_6F_2$ crystal structure along [001] axis is illustrated in Fig. 1(b). As shown, there are two nonequivalent cation sites, the seven-coordinated 6h (C_s) site [La^{3+}/Ba^{2+}(II)] and the nine-coordinated 4f (C_3) site [La^{3+}/Ba^{2+}(I)], which are connected by isolated $[SiO_4]^{4-}$ tetrahedrons. The $[SiO_4]^{4-}$ tetrahedrons, La/Ba(I) polyhedrons and La/Ba(II) polyhedrons form the framework structure of the $La_6Ba_4(SiO_4)_6F_2$ host.

The SEM micrograph of the LBSF:0.12Dy^{3+} phosphor is shown in Fig. 1(c). The typical microstructure of the sample shows the inherent characteristic results from the solid-state reaction method. The particles are irregular in shape, and the synthesized and ground phosphor has a wide particle size distribution range from 1 to 10 μm. In Fig. 1(c), the elemental mapping of LBSF: 0.12Dy^{3+} phosphor is shown. In the final product, the constituent elements La, Ba, Si, O, F and Dy are uniformly distributed over the whole observed area. Based on these results, the phosphor mostly can meet the fabrication requirements for w-LEDs. Furthermore, it is noticed that the particles are closely packed, which helps to prevent light scattering. Therefore, more efficient light output can be obtained.[35] In addition, by using EDS for LBSF phosphor, we accomplished elemental analysis and have identified the elements, *i.e.*, Ba, La, Si, O, F in the proportions as seen in the EDS spectrum, respectively. The elemental composition of the sample is shown in Table 1.

3.2. Luminescence properties of LBSF:Dy^{3+}

At different Dy^{3+} concentrations, we tested the luminescence properties of LBSF samples at RT. In Fig. 2(a) and (b), the emission (λ_{em} = 579 nm) and excitation spectra (λ_{ex} = 353 nm) are displayed, respectively. The excitation spectrum shown in Fig. 2(b) exhibited four intense bands centered at the wavelengths of 300, 327, 353 and 389 nm, corresponding to the transitions $^6H_{15/2} \rightarrow {}^6P_{3/2}$, $^6H_{15/2} \rightarrow {}^6P_{7/2}$, $^6H_{15/2} \rightarrow {}^6P_{5/2}$ and $^6H_{15/2} \rightarrow {}^4I_{13/2}$ (389 nm), one moderate band at 454 nm and one weak band at 427 nm, due to $^6H_{15/2} \rightarrow {}^4I_{15/2}$ and $^6H_{15/2} \rightarrow {}^4G_{11/2}$ transitions, respectively. The PLE peaks for Dy^{3+} doped $La_6Ba_4(SiO_4)_6F_2$ phosphor offer a great opportunity for WLED devices with excitation using blue InGaN/GaN LED chips.[36] In Fig. 2(b), at 353 nm excitation, when the Dy^{3+} concentration increases from 0.03 to 0.30 mol, the emission intensity initially increases and then decreases due to the concentration quenching (CQ) phenomena. In LBSF doped with Dy^{3+} ions, the

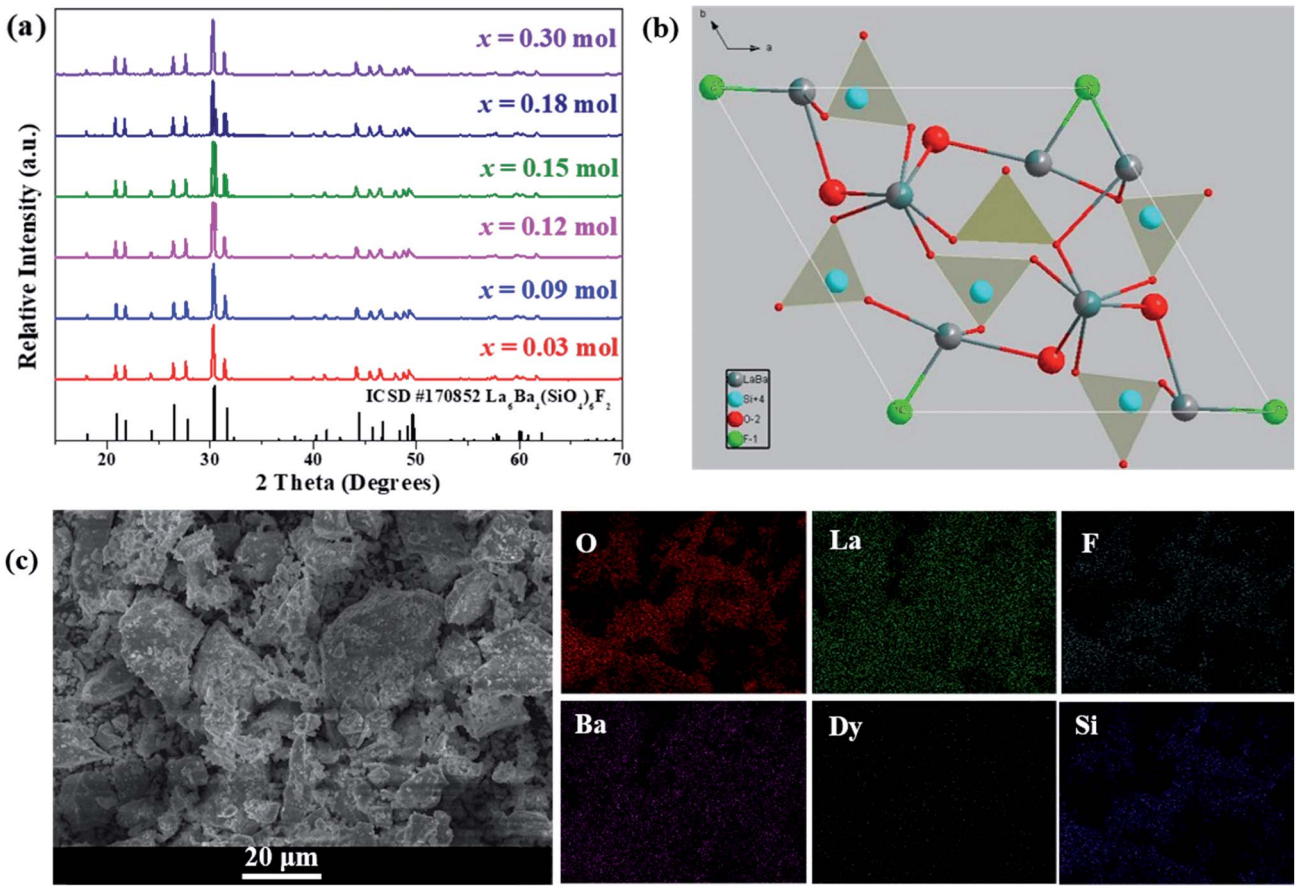

Fig. 1 (a) XRD patterns of LBSF:xDy^{3+} (x = 0.30, 0.18, 0.15, 0.12, 0.09 and 0.03) samples, (b) crystal structure of the host LBSF compound viewed along the c axis, (c) the SEM micrograph of LBSF:0.12Dy^{3+} phosphor and the elemental mapping of LBSF:Dy^{3+} phosphors.

optimal doping concentration was 0.12 mol.[37] Because of partial crystal field degeneracy around the Dy^{3+} ions, the blue emission bands are split into two components. Due to the Stark effect enhancement and increase in Dy^{3+} concentration, the crystal-field splitting increases. The main emission band at 579 nm corresponds to the $^4F_{9/2} \rightarrow {}^6H_{13/2}$ transition known as the electric dipole transition or hypersensitive transition, and the one at 484 nm originates due to the $^4F_{9/2} \rightarrow {}^6H_{15/2}$ transition known as the magnetic dipole transition, which usually shows lower intensity than the electric dipole transition.[38–40] The variation of the Y/B, yellow-to-blue luminescence, intensity ratio is applicable to white light emission with Dy^{3+} ions tuning the yellow and blue components. In Table 2, the Y/B values for LBSF with different dysprosium concentrations are listed. As seen, the Y/B ratios are practically insensitive to the concentration of Dy^{3+} ions. Evidently, larger Y/B values are observed for higher concentration of dysprosium. Based on this trend, we validate that the Y/B ratio increases at low concentrations of Dy^{3+} ions in the $La_6Ba_4(SiO_4)_6F_2$ system. The maximum value of Y/B is 1.03 for LBSF:0.15Dy^{3+}, showing a good agreement with the concentration dependence of PL, as shown in Fig. 2(b). It can be assumed that the small changes in the Y/B ratios are caused by structural changes near the Dy^{3+} ions.[41–44] The results show that the Dy^{3+} ions occupy lower symmetry sites in the LBSF structure, as indicated by the XRD results.

Table 1 The elemental composition of the host $La_6Ba_4(SiO_4)_6F_2$ sample determined by EDS analysis

Element	Weight%	Atomic%
O	19.86	58.72
F	2.24	5.60
Si	6.71	11.33
Ba	28.17	9.70
La	43.01	14.65
Totals	100.00	

3.3. Decay characteristics

In Fig. 3, the fluorescence decay curves of the Dy^{3+} emission are shown for the LBSF:Dy^{3+} phosphors, as excited at 350 nm and monitored at 573 nm. The decay curves can be properly fitted by a second order exponential equation:[45]

$$I(t) = I_1 \exp\left(-\frac{t}{\tau_1}\right) + I_2 \exp\left(-\frac{t}{\tau_2}\right) \quad (1)$$

in which I stands for the phosphorescent intensity. I_1, I_2 are intensity constants, τ represents the time, and τ_1, τ_2 are the fast and slow lifetimes for exponential components. The

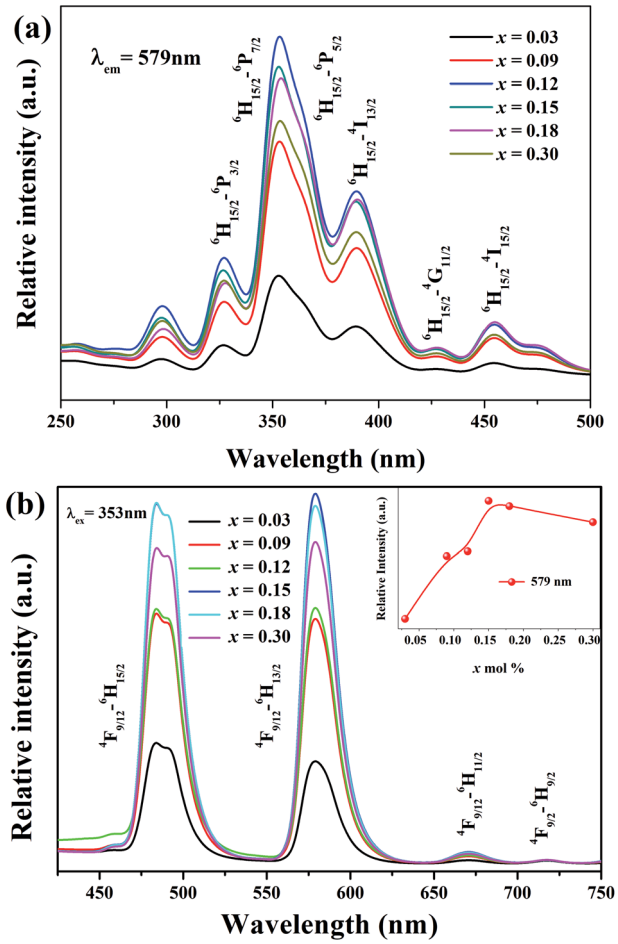

Fig. 2 (a) The PL excitation (PLE) spectra (λ_{em} = 579 nm) of LBSF:xDy^{3+}, (b) the PL emission spectra (λ_{ex} = 353 nm) of LBSF:xDy^{3+}, and the inset in (b) shows the variable 579 nm peak intensity with increasing dopant concentration.

determined lifetime values and fitting parameters are given in Table 3. The $^4F_{9/2}$ luminescence lifetime depends on the concentration of Dy^{3+} ions. With the enhancement of Dy^{3+} dopant concentration, the typical values of lifetime shorten from about 0.76 to 0.4 ms, as expected. We find that the effective lifetimes decrease with increasing Dy^{3+} concentration, and energy transfer to Dy^{3+} ions through cross-relaxation processes and energy transfer between luminescence quenching centers and impurities are the probable reasons.[44,46]

3.4. Energy transfer process

Generally, with increasing Dy^{3+} concentration, the relative distance between the Dy^{3+} luminescent centers decreases. This promotes nonradiative energy transfer between adjacent Dy^{3+} ions, leading to concentration quenching at high dopant concentrations. In the energy transfer process, there could be quenching sites where the excitation energy dissipates, resulting in luminescence quenching. To check the concentration quenching mechanism, it is necessary to determine the critical distance (R_C) between the Dy^{3+} ions. R_C can be evaluated on the basis of the Blasse equation:[47,48]

Table 2 The (Y/B) intensity ratios of luminescence spectra evaluated and the calculated chromaticity coordinates for the white light emitted from LBSF:xDy^{3+} phosphor (x = 0.03, 0.09, 0.12, 0.15, 0.18, 0.3)

Sample no.	C	484	579	Y/B ratio	(x, y)
1	0.03	901.3	764.8	0.85	(0.3032, 0.3371)
2	0.09	1860	1821	0.98	(0.3298, 0.3646)
3	0.12	1895	1902	1.00	(0.3206, 0.3496)
4	0.15	2675	2749	1.03	(0.3422, 0.3780)
5	0.18	2681	2659	0.99	(0.3391, 0.3765)
6	0.30	2345	2390	1.02	(0.3403, 0.3768)

$$R_C \approx 2\left(\frac{3V}{4\pi x_c N}\right)^{1/3} \quad (2)$$

in which V is the volume belonging to the unit cell, x_c is the critical concentration of Dy^{3+}, N represents the formula units per unit cell. Taking appropriate values of V, x_c, and N (10, 608.77 Å^3, 0.12, respectively) for LBSF:0.12Dy^{3+} phosphor, R_C is estimated to be about 9.89 Å. Consequently, it is deduced that the exchange interaction contribution to concentration quenching effect is inefficient in the LBSF system since exchange interaction occurs when R_C is smaller than 5 Å.[49] Therefore, in the case of Dy^{3+}, the concentration quenching mechanism was dominated by the multipolar–multipolar interaction. This model of energy transfer between similar activators, as well as the relation between Dy^{3+} concentration and the luminescence intensity is pointed out on the basis of Dexter theory. As given by the equation below, there is a relation between activator concentration (x) and luminescence intensity (I):[50,51]

$$\frac{I}{x} = K\left[1 + \beta(x)^{\theta/3}\right]^{-1} \quad (3)$$

where x is the activator concentration, θ is a multipolar interaction constant equal to 3, 6, 8 or 10 corresponding to the nearest-neighbor ions, which means dipole–dipole (d–d), dipole–quadrupole (d–q), and quadrupole–quadrupole (q–q)

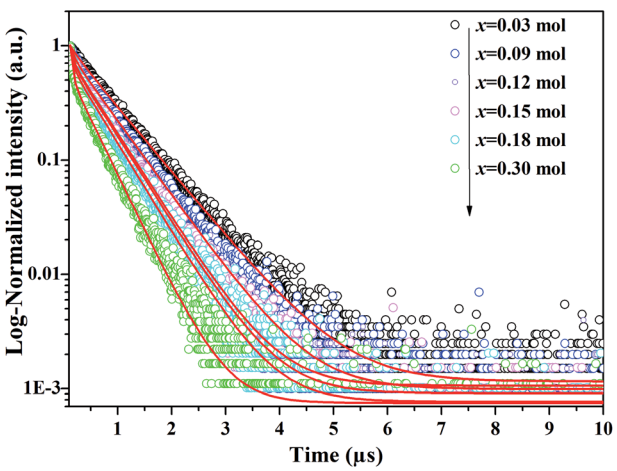

Fig. 3 Decay curves of Dy^{3+} emission for LBSF:xDy^{3+} phosphors under excitation 353 nm, monitored at 579 nm.

Table 3 Determined luminescence lifetimes and fitting parameters for the LBSF:xDy^{3+} samples

Sample no.	C (mol)	τ_1 (ms)	A_1 (%)	τ_2 (ms)	A_2 (%)	$\tau_{average}$ (ms)	R^2
1	0.03	0.7644	94.38%	0.1976	5.62%	0.76	0.9983
2	0.09	0.0740	10.95%	0.6620	89.05%	0.65	0.9982
3	0.12	0.5864	80.44%	0.0498	19.56%	0.58	0.9980
4	0.15	0.5767	75.88%	0.0585	24.12%	0.56	0.9977
5	0.18	0.0443	31.98%	0.5559	68.02%	0.54	0.9976
6	0.30	0.4400	42.03%	0.0343	57.97%	0.40	0.9967

interactions, respectively,[52] and K and β are constants for each interaction at the same excitation. Exceeding the quenching concentration, we chose the LBSF:0.15, 0.18, 0.27, 0.3Dy^{3+} samples for consistent emission intensity measurements at 484 nm. As seen in Fig. 4, by the $\log(I/x) - \log(x)$ plot, the value of θ is determined to be 6.07 for the peak at 484 nm. Thus, for concentration quenching in the system under consideration, the dipole–dipole (d–d) interaction is dominant.

3.5. CIE chromaticity coordinate

As one of the important factors, the CIE, Commission International de I'Eclairage[53] 1931, is widely used to ascertain the chromaticity coordinates and evaluate the phosphor performance. The chromaticity coordinates of LBSF:Dy^{3+} phosphors with different dopant concentrations under UV excitation at 353 nm are listed in Table 2. The LBSF:Dy^{3+} samples on the CIE chromaticity diagram are shown in Fig. 5. As evident, all LBSF:Dy^{3+} samples are in the white region. Moreover, the point of LBSF:0.12Dy^{3+} phosphor, ($x = 0.3206$, $y = 0.3496$), is very close to standard white light ($x = 0.334$, $y = 0.337$).[54] Hence, the present results imply that the LBSF:0.12Dy^{3+} phosphor could have a likely application for white light-emitting diodes.

3.6. Temperature-dependent luminescence properties

For long-term operation, w-LED chip temperatures could increase up to 150 °C, so, the thermal stability of the phosphors is one of the most vital issues for their applications in high-powered LEDs.[55] In Fig. 6, the temperature-dependent emission spectra of the LBSF:0.12Dy^{3+} phosphor excited at 353 nm is shown for the temperature range from RT to 250 °C. The PL relative intensity decreases gradually with increasing temperature and it remains above 60% at 150 °C, reflecting that the prepared phosphor has high thermal stability. A plot of the luminescence intensity *vs.* temperature is shown in the inset of Fig. 6. Currently, during the LED operation, due to the heat generated by the LED itself, the temperature is up to 150 °C for a long time and the phosphors should maintain their emission efficiency. It is observed that in LBSF:0.12Dy^{3+} phosphor the Dy^{3+} luminescence intensity related to the $^4F_{9/2}$ to $^6H_{15/2}$ and $^4F_{9/2}$ to $^6H_{13/2}$ transitions reaches 62.03% and 67.28%, respectively, when the temperature is elevated up to 150 °C, as compared to the room temperature parameters. Because of non-radiative relaxation through the excited state and its crossover to the ground state, the thermal quenching effect, where the probability of non-radiative transition strictly relies on the temperature causes PL quenching of Dy^{3+} emission at high temperatures. The relationship between the temperature and

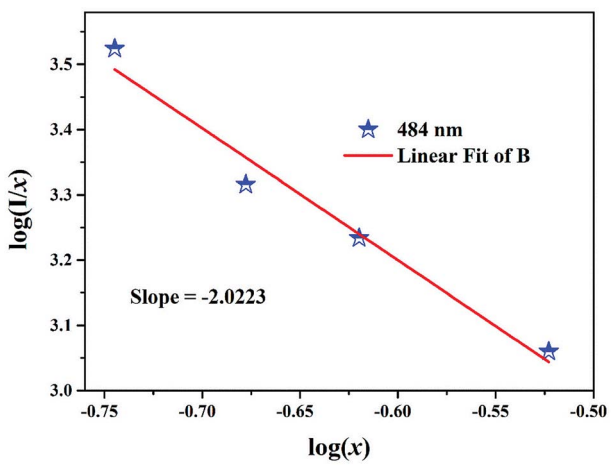

Fig. 4 Relationship between the log(I/x) and log(x) of Dy^{3+} content in LBSF:xDy^{3+} phosphors beyond the quenching concentration ($x = 0.15$, 0.18, 0.27, 0.3).

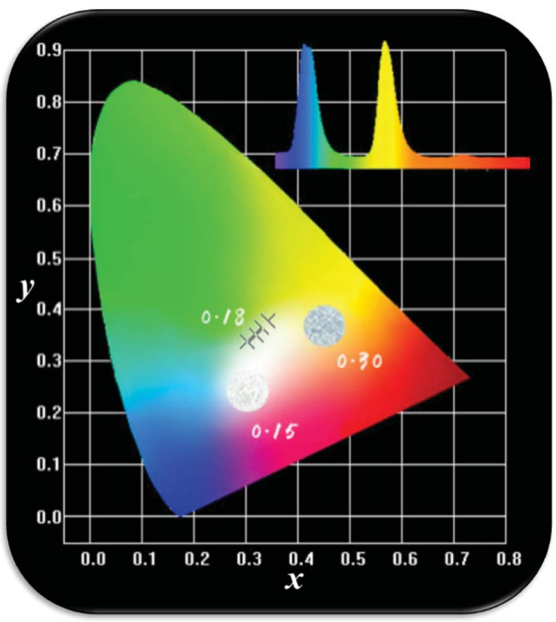

Fig. 5 The CIE chromaticity coordinates (x, y) LBSF:xDy^{3+} samples, and the corresponding images of samples luminescence under UV light irradiation.

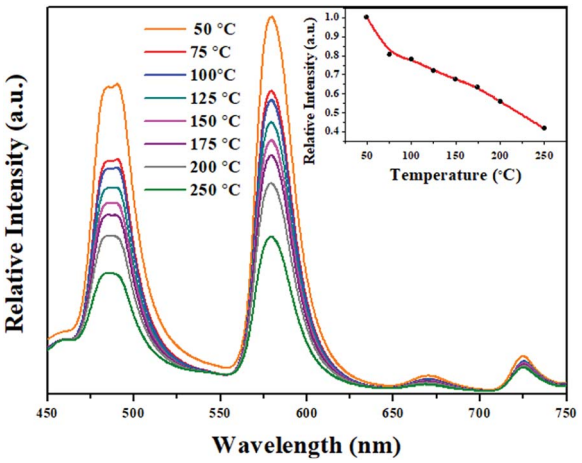

Fig. 6 Emission spectra of LBSF:0.12Dy^{3+} under 353 nm excitation at different temperatures, and the inset shows the PL intensity as a function of temperature.

photoluminescence intensity could be described with a modified Arrhenius equation:[56–58]

$$I(T) \approx \frac{I_0}{1 + c\exp\left(\frac{-E}{kT}\right)} \quad (4)$$

where $I(T)$ is the intensity at temperature T, I_0 is the initial intensity, c is a constant, E is the activation energy between the bottom of the excited state $^4F_{9/2}$ and its crossover point to the ground state $^6H_{13/2}$ and k is the Boltzmann constant. For the present LBSF:0.12Dy^{3+} phosphor, Fig. 7 gives evidence of the emission thermal quenching model fitting line plotted as $\ln(I_0/I) - 1$ against $1/kT$. As revealed by the fitting with eqn (4), the activation energy value E is equal to 0.154 eV for the $^4F_{9/2}$ to $^6H_{13/2}$ transition of Dy^{3+} ions. Therefore, the obtained LBSF:0.12Dy^{3+} phosphor shows good thermal stability, which offers an excellent possibility for application in w-LEDs. The chromaticity coordinates of LBSF:0.12Dy^{3+} phosphors at different temperatures ranging from RT to 250 °C under 353 nm excitation are shown in Table 4. As shown in Table 4, the

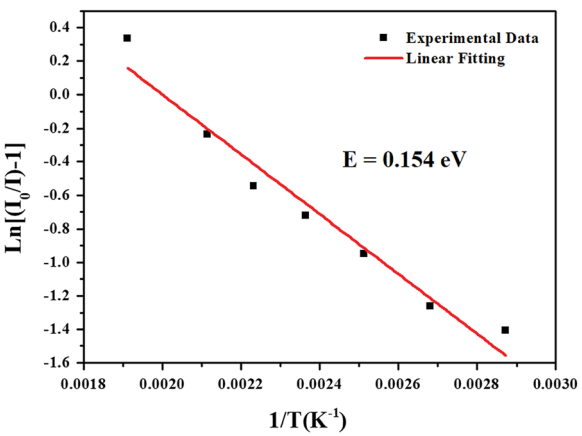

Fig. 7 The fitting line of the emission thermal quenching model plotted as $\ln(I_0/I) - 1$ against $1/kT$ for the present LBSF:0.12Dy^{3+} phosphor.

Table 4 The chromaticity coordinates of LBSF:0.12Dy^{3+} phosphor at different temperatures ranging from RT to 250 °C under 353 nm excitation

Sample no.	Temperature (°C)	(x, y)
1	RT	(0.3285, 0.3538)
2	75	(0.3296, 0.3473)
3	100	(0.3290, 0.3461)
4	125	(0.3277, 0.3437)
5	150	(0.3261, 0.3412)
6	175	(0.3241, 0.3397)
7	200	(0.3182, 0.3320)
8	250	(0.3043, 0.3161)

chromaticity coordinates of LBSF:0.12Dy^{3+} phosphors at different temperature ranging from RT to 250 °C under 353 nm excitation are stable, and are all located in white region.

4. Conclusion

In conclusion, by using the traditional solid-state reaction method, the new feasible single-phased white light-emitting $La_{6-x}Ba_4(SiO_4)_6F_2$:Dy^{3+} phosphors were synthesized favorably. Subsequently, we reported on the systematic study of the crystal structure, morphology and luminescence performance of prepared samples. The XRD patterns confirmed their phase purity, and that the compounds belong to the apatite family. SEM measurement demonstrated a closely packed particle morphology. Under UV excitation, two intense characteristic bands *i.e.* blue bands at 484 nm, yellow bands at 579 nm, corresponding to transitions of Dy^{3+}, $^4F_{9/2} \rightarrow {}^6H_{15/2}$ and $^4F_{9/2} \rightarrow {}^6H_{13/2}$, respectively, dominate the photoluminescence spectra accompanied by a weak red band at 670 nm, contributing to $^4F_{9/2} \rightarrow {}^6H_{11/2}$. The concentration quenching mechanism of the Dy^{3+} ions is controlled by a dipole–dipole interaction, and the optimal dopant concentration of Dy^{3+} in the $La_{6-x}Ba_4(SiO_4)_6F_2$ host was determined to be 0.12 (mol). The critical transfer distance between the Dy^{3+} ions is calculated to be 9.89 Å. In the CIE diagram, the emission color of $La_6Ba_4(SiO_4)_6F_2$:Dy^{3+} phosphors falls in the white light zone. Furthermore, thermal quenching measurements indicate excellent thermal stability. Combining all the results, we can indicate that $La_6Ba_4(SiO_4)_6F_2$:Dy^{3+} may serve as white light-emitting phosphors for white-light-emitting diodes (w-LEDs).

Conflicts of interest

There are no conflicts to declare.

Acknowledgements

The study was supported by the National Natural Science Foundations of China 277 (Grant No. 51672257) and the Fundamental Research Funds for the Central Universities (Grant No. 2652017094 and 2652017091). Jialei Zhang also express thanks to the supporting from the College Student Research Innovation Program of China University of Geosciences, Beijing.

References

1 X. X. Ma, L. B. Liao, Q. F. Guo, H. K. Liu, T. S. Zhou and L. F. Mei, *RSC Adv.*, 2018, **8**, 27332–27341.
2 Q. F. Guo, Q. D. Wang, L. W. Jiang, L. B. Liao LB, H. K. Liu and M. F. Mei, *Phys. Chem. Chem. Phys.*, 2016, **118**, 15545–15554.
3 M. F. Zhang, Y. J. Liang, S. Y. Xu, Y. L. Zhu, X. Y. Wu and S. Q. Liu, *RSC Adv.*, 2016, **18**, 68–76.
4 X. C. Wang and Y. H. Wang, *J. Phys. Chem. C*, 2015, **119**(28), 16208–16214.
5 V. V. Atuchin, N. F. Beisel, E. N. Galashov, E. M. Mandrik, M. S. Molokeev, A. P. Yelisseyev, A. A. Yusuf and Z. G. Xia, *ACS Appl. Mater. Interfaces*, 2015, **7**, 26235–26243.
6 H. P. Ji, L. Wang, M. S. Molokeev, N. Hirosaki, R. J. Xie, Z. H. Huang, Z. G. Xia, O. M. T. Kate, L. H. Liu and V. V. Atuchin, *J. Mater. Chem. C*, 2016, **4**, 6855–6863.
7 E. N. Galashov, V. V. Atuchin, T. A. Gavrilova, I. V. Korolkov, Y. M. Mandrik, A. P. Yelisseyev and Z. G. Xia, *J. Mater. Sci.*, 2017, **52**(22), 13033–13039.
8 M. F. Zhang, Y. J. Liang, R. Tang, D. Y. Yu, M. H. Tong, Q. Wang, Y. L. Zhu, X. Y. Wu and G. G. Li, *RSC Adv.*, 2014, **4**, 40626–40637.
9 Y. L. Zhu, Y. J. Liang, M. F. Zhang, M. H. Tong, G. G. Li and S. Wang, *RSC Adv.*, 2015, **5**, 98350–98360.
10 H. Choi, C. H. Pyun and S.-J. Kim, *J. Lumin.*, 1999, **82**, 25–32.
11 H. K. Liu, L. B. Liao, Q. F. Guo, D. Yang and L. F. Mei, *J. Lumin.*, 2017, **181**, 407–410.
12 Q. Su, H. Liang, C. Li, H. He, Y. Lu, J. Li and Y. Tao, *J. Lumin.*, 2007, **122–123**, 927–930.
13 B. Han, H. Liang, H. Lin, W. Chen, Q. Su, G. Yang and G. Zhang, *J. Opt. Soc. Am. B*, 2008, **25**, 2057–2063.
14 S. H. Liu, J. Y. He, Z. Y. Wu, J. H. Jeong, B. Deng and R. Yu, *J. Lumin.*, 2018, **200**, 164–168.
15 G. Tiwari, N. Brahme, R. Sharma, D. P. Bisen, S. K. Sao and S. Tigga, *Opt. Mater.*, 2016, **58**, 234–242.
16 H. K. Liu, L. B. Liao, M. S. Molokeev, Q. F. Guo, Y. Y. Zhang and L. F. Mei, *RSC Adv.*, 2016, **6**, 24577–24583.
17 V. Kumar, M. Manhas, A. K. Bedyal and H. C. Swart, *Mater. Res. Bull.*, 2017, **91**, 140–147.
18 R. Vijayakumar, H. Guo and X. Y. Huang, *Dyes Pigm.*, 2018, **156**, 8–16.
19 J. Y. Wang, J. B. Wang and P. Duan, *Mater. Lett.*, 2013, **107**, 96–98.
20 X. H. Zhang, Z. M. Lu, F. B. Meng, F. Lu, L. Hu, X. W. Xu and C. C. Tang, *Mater. Lett.*, 2012, **66**, 16–18.
21 Q. Guo, B. Ma, L. Liao, M. S. Molokeev, L. Mei and H. Liu, *Ceram. Int.*, 2016, **42**, 11687–11691.
22 K. Li, D. L. Geng, M. M. Shang, Y. Zhang, H. Z. Lian and J. Lin, *J. Phys. Chem. C*, 2014, **118**, 11026–11034.
23 L. E. Muresan, I. Perhaita, D. Prodan and G. Borodib, *J. Alloys Compd.*, 2018, **755**, 135–146.
24 P. Ptáček, T. Opravil, F. Šoukal, J. Tkacz, J. Másilko and E. Bartoníčková, *Ceram. Int.*, 2016, **42**, 6154–6167.
25 H. Njema, K. Boughzala, A. Chaabe` ne and K. Bouzouita, *C. R. Chim.*, 2014, **17**, 1237–1241.
26 F. Zhang and B. T. Liu, *J. Alloys Compd.*, 2012, **542**, 276–279.
27 J. Felsche, *J. Solid State Chem.*, 1972, **5**, 266–275.
28 X. Lu, H. T. Liu, X. Y. Yang, Y. G. Tian, X. L. Gao, L. Y. Han and Q. Xu, *Ceram. Int.*, 2017, **43**, 11686–11691.
29 S. Lahrich, M. A. Elmhammedi, B. Manoun, Y. Tamraoui, F. Mirinioui, M. Azrour and P. Lazor, *Spectrochim. Acta, Part A*, 2015, **145**, 493–499.
30 X. H. Gong, Y. F. Lin, Y. J. Chen, Z. X. Huang, Y. D. Huang and Z. D. Luo, *Chem. Mater.*, 2005, **17**, 1135–1138.
31 H. Ye, M. Y. He, T. S. Zhou, Q. F. Guo, J. L. Zhang, L. B. Liao, L. F. Mei, H. K. Liu and M. Runowskid, *J. Alloys Compd.*, 2018, **757**, 79–86.
32 J. M. Hughes and M. Cameron, *Am. Mineral.*, 1991, **76**, 1165–1173.
33 Q. F. Guo, L. B. Liao and Z. G. Xia, *J. Lumin.*, 2014, **145**, 65–70.
34 X. Gong, Y. Lin, Y. Chen, Z. Huang, Y. Huang and Z. Luo, *J. Mater. Chem.*, 2005, **17**, 1135–1138.
35 V. P. Tishkovets, *J. Quant. Spectrosc. Radiat. Transfer*, 2008, **109**, 2665–2672.
36 L. L. Devi, C. Basavapoornima, V. Venkatramu, P. Babu and C. K. Jayasankar, *Ceram. Int.*, 2017, **43**, 16622–16627.
37 A. K. Parchur and R. S. Ningthoujam, *Dalton Trans.*, 2011, **40**, 7590–7594.
38 S. N. Ogugua, H. C. Swart and O. M. Ntwaeaborwa, *Phys. B*, 2016, **480**, 131–136.
39 J. B. Gruber, B. Zandi, U. V. Valiev and Sh. A. Rakhimov, *J. Appl. Phys.*, 2003, **94**(2), 1030–1034.
40 K. N. Shinde, S. J. Dhobe and A. Kumar, *J. Lumin.*, 2011, **131**, 931–937.
41 J. Pisarska, R. Lisiecki, W. Ryba-Romanowski, T. Goryczka and W. A. Pisarski, *Chem. Phys. Lett.*, 2010, **489**, 198–201.
42 S. Ruengsri, S. Insiripong, N. Sangwaranatee, H. J. Kim, N. Wantana, A. Angnanon and J. Kaewkhao, *Integr. Ferroelectr.*, 2017, **177**, 39–47.
43 U. Fawad, M. Oh, H. Park, S. Kim and H. J. Kim, *J. Alloys Compd.*, 2014, **610**, 281–287.
44 P. Haritha, I. R. Martín, K. Linganna, V. Monteseguro, P. Babu, S. F. León-Luis, C. K. Jayasankar, U. R. Rodríguez-Mendoza, V. Lavín and V. Venkatramu, *J. Appl. Phys.*, 2014, **116**, 174308.
45 C. H. Huang and T. M. Chen, *J. Phys. Chem. C*, 2011, **115**, 2349–2355.
46 P. Haritha, I. R. Martín, C. S. Dwaraka Viswanath, N. Vijaya, K. Venkata Krishnaiah, C. K. Jayasankar, D. Haranath, V. Lavín and V. Venkatramu, *Opt. Mater.*, 2017, **70**, 16–24.
47 G. Blasse, *Philips Res. Rep.*, 1969, **24**, 131–144.
48 J. H. Chen, W. R. Zhao, J. Q. Wang, N. H. Wang, Y. J. Meng, J. He and X. Zhang, *Ceram. Int.*, 2015, **41**, 11945–11952.
49 R. Vijayakumar, H. Guo and X. Y. Huang, *Dyes Pigm.*, 2018, **156**, 8–16.
50 C. H. Huang, T. W. Kuo and T. M. Chen, *ACS Appl. Mater. Interfaces*, 2010, **2**(5), 1395–1399.
51 L. G. Van Uitert, *J. Electrochem. Soc.*, 1967, **114**, 1048–1053.
52 D. L. Dexter and J. H. Schulman, *J. Chem. Phys.*, 1954, **22**, 1063–1070.
53 J. S. Kumar, K. Pavani, A. M. Babu, N. K. Giri, S. B. Rai and L. R. Moorthy, *J. Lumin.*, 2010, **130**, 1916–1923.

54 S. Fan, C. Yu, D. He, X. Wang and L. Hu, *Opt. Mater. Express*, 2012, **6**, 765–770.
55 T. Takeda, N. Hirosaki, S. Funahshi and R. Xie, *Chem. Mater.*, 2015, **27**, 5892–5898.
56 W. Xiao, X. Zhang, Z. Hao, G. Pan, Y. Luo and L. Zhang, *Inorg. Chem.*, 2015, **54**, 3189–3195.
57 S. Xin and G. Zhu, *RSC Adv.*, 2016, **6**, 41755–41760.
58 L. Chen, R. Liu, W. Zhuang, Y. Liu, Y. Hu and X. Zhou, *CrystEngComm*, 2015, **17**, 3687–3694.